International Journal of Environmental Science and Technology (2024) 21:6429–6444
https://doi.org/10.1007/s13762-024-05464-4

ORIGINAL PAPER

Microstructure development in lacustrine, fine-grained sediments traced by in situ and laboratory testing

S. Oberhollenzer[1,4] · L. Hauser[1] · A. Baldermann[2] · R. Marte[1] · F. Tschuchnigg[1] · H. F. Schweiger[1] · M. Nachtnebel[3] · M. Dietzel[2]

Received: 2 May 2023 / Revised: 3 January 2024 / Accepted: 7 January 2024 / Published online: 28 February 2024

Abstract

Soil microstructure, often defined as the combination of particle arrangement and bonding, can strongly influence the stiffness and strength of sedimentary deposits. As undisturbed soil sampling is a challenging task in fine-grained soils, seismic in situ testing is becoming increasingly more important to investigate its mechanical behaviour. The aim of this article is to evaluate the influences of sediment depositional age and structure-forming processes on the degree of soil structure development in Alpine deposits. Seismic in situ and laboratory testing comprising X-ray diffraction (XRD), scanning electron microscopy (SEM), pore water chemical analysis and hydrochemical modelling were executed at three Austrian test sites, namely *Lokalbahn Salzburg*, *Rhesi* and *water reservoir Raggal*. Based on the comparison of in situ shear wave velocities ($V_{S,\mathrm{SDMT}}$) with bender element results ($V_{S,\mathrm{BE}}$), executed on reconstituted soil specimens, it is shown that the Pleisto–Holocene-aged deposits are characterized by a $V_{S,\mathrm{BE}}/V_{S,\mathrm{SDMT}}$ ratio of <1, indicating the presence of microstructure. However, the youngest sediments (<50 years) exhibit the weakest microstructure ($V_{S,\mathrm{BE}}/V_{S,\mathrm{SDMT}} \approx 1$). The increase of soil structure with sediment age is represented by the updated normalized small-strain rigidity index, K^*_G, which is situated at the proposed transition between structured and unstructured soils ($K^*_G = 330$), ranging between 250 and 350, at all test sites. The development of microstructure can be attributed to the precipitation of calcite ($CaCO_3$) cements in open pores, which strengthens the interparticle bonding between detrital quartz, feldspar, clay minerals and carbonate grains, subsequently reducing the soil`s porosity with increasing sediment age.

Keywords Lacustrine sediments · Microstructure · Direct push downhole seismic test · Bender element test · Carbonate cementation · Pore water composition

Introduction

Fine-grained (pelitic) sediments dominate the soil layering of various Alpine basins and valleys. Many of these basins were formed during several glacial–interglacial periods of the Pleistocene and Holocene and remained as lakes after the last glaciation (van Husen 1979). Lacustrine sediments have filled the basins over thousands of years and are usually characterized by high groundwater tables nowadays. These sediments can lead to an increased risk for building settlements due to their moderate stiffness and strength properties (Petry and Little 2022), leading to high costs for foundation and construction works due to large or differential settlements (Marte and Oberhollenzer 2022). In contrast, it was observed at different construction sites that soft postglacial deposits may be characterized by an unexpectedly high stiffness, leading to small building settlements on shallow

Editorial responsibility: Jing Chen.

✉ S. Oberhollenzer
s.oberhollenzer@tugraz.at

1 Institute of Soil Mechanics, Foundation Engineering and Computational Geotechnics, Graz University of Technology, Rechbauerstraße 12, 8010 Graz, Austria

2 Institute of Applied Geosciences, Graz University of Technology and NAWI Graz Geocenter, Rechbauerstraße 12, 8010 Graz, Austria

3 Graz Centre for Electron Microscopy (ZFE), Steyrergasse 17, 8010 Graz, Austria

4 Norwegian Geotechnical Institute (NGI), Onshore Foundations, Sandakerveien 140, 0484 Oslo, Norway

foundations. Therefore, geotechnical engineers often assume that most (pelitic) soils have a distinct structure (i.e. defined as the combination of particle arrangement and bonding), which may lead to increased soil stiffness and strength properties.

Soil particle characteristics (e.g. size, shape, mineralogical composition), as well as their arrangement and interparticle bonds, significantly influence soil compressibility, strength and permeability (Leroueil and Vaughan 1990; Mitchell 1976). Here, the term *fabric* is used to describe the arrangement of particles and pore spaces in pelitic soils. Mitchell (1976) and Burland (1990) introduced the term *structure* to describe the effects of particle arrangement (fabric) and bonding. Consequently, soils that are characterized by the same fabric can exhibit different properties in terms of stiffness and strength due to different degrees of interparticle bonding. Significant modifications of the original soil structure can, for example, result from the use of inadequate sampling techniques, leading to a reduction in stiffness and strength of the destructed (or *non-structured*) soil compared to the natural state (Cotecchia and Chandler 2000). While the initial structure is fully lost for *remoulded* specimens, artificially prepared specimens are named *reconstituted* (Fearon and Coop 2000). Indeed, natural and reconstituted soils differ significantly with respect to their fabric and particle bonding since compositional factors (e.g. soil particle mineralogy, size and shape), environmental factors (e.g. pore water composition, pressure, temperature and weathering regimes), chemical processes (e.g. leaching, cementation, oxidation and mineral alteration), physical processes (e.g. consolidation, freezing and thawing) and biological processes (e.g. microbial activity, burrowing and production and decay of organic matter) influence the soil`s structure. Consequently, the origin and formation of soil structure may differ between locations (Leroueil and Vaughan 1990), although Tavenas and Leroueil (1980) argue that most natural soils exhibit some structure.

An improved characterization of soil structure(s) is therefore required (i) to capture the mechanical properties of natural soils and assess their changes during construction, (ii) to optimize existing construction measures (e.g. excavation support and foundation systems) and (iii) to introduce sustainable construction concepts, such as long-term carbon binding and sequestration (e.g. shallow carbon storage) in soft soils. While the structure of marine and lacustrine sediments was studied at various locations (Cotecchia et al. 2007, Tsige et al. 1994, Nespereira et al. 2021), only a few investigations have been executed in normally consolidated Alpine deposits. In this article, the degree and origin of soil structure development in pelitic sediments are investigated at three test sites in Austria, namely *Lokalbahn Salzburg*, *Rhesi* and *water reservoir Raggal*, using in situ and laboratory testing based on recovered soil and pore water samples.

Materials and methods

In situ testing

Piezocone penetration tests (*CPTu*) were used for site characterization, including soil profiling at the three test sites. During test execution, the tip resistance q_c, the sleeve friction f_s and the dynamic pore water pressure u_2 were measured. The dynamic pore water pressure u_2 was obtained at the shoulder of the cone. A 15 cm^2 cone with a tip opening angle of 60° was pushed into the soil at a constant penetration rate of 2 ± 0.5 cm/s using a hydraulic unit in combination with 1–m-long penetration rods. The testing procedure is standardized following ISSMGE (IRTP 1999) and several national standards (e.g. ISO 22476-1 2012, ASTM D5778-12 2012). In the present work, all *CPTu* were executed according to ISO 22476-1.

As q_c is affected by u_2, generated at the shoulder of the cone, Jamiolkowski et al. (1985) suggested using u_2 to determine the corrected tip resistance q_t based on Eq. (1):

$$q_t = q_c + (1 - a) \cdot u_2 \tag{1}$$

where a is the cone area ratio, usually ranging between 0.8 and 0.9. Since the in situ stress state strongly influences the in situ measurements, Robertson (2009) introduced the updated normalized tip resistance Q_{tn} and the normalized friction ratio F_r for *CPTu*-based soil classification as summarized by Eqs. (2) and (3):

$$Q_{tn} = \frac{(q_t - \sigma_{v0})}{p_a} \cdot \left(\frac{p_a}{\sigma'_{v0}}\right)^n \tag{2}$$

$$F_r = \frac{f_s}{q_t - \sigma_{v0}} 100\% \tag{3}$$

where σ_{v0} and σ'_{v0} are the in situ total and effective vertical stresses, respectively, and p_a represents the atmospheric pressure. The stress exponent n was calculated based on the soil behaviour type index I_C (Robertson 2016).

Direct push downhole seismic tests (*DPDH*) were performed by penetrating a seismic module, equipped with geophones, into the soil. The advanced system by Marchetti et al. (2008), which consists of two geophones installed at a vertical distance of 50 cm, was mounted between the penetration rods and the flat dilatometer blade (DMT) and allowed for measuring the shear wave velocity V_S. Therefore, penetration was stopped at regular intervals for V_S measurements. The seismic wave, triggered by a hammer blow and received by both geophones, was amplified, digitized and send to the computer for data interpretation (Marchetti et al. 2008). The true interval interpretation method, described in more detail by Marchetti et al. (2008), was used to determine

V_S. For each testing depth (~50 cm intervals), three repeated seismic measurements were performed and averaged for data interpretation. The individual V_S measurements at defined testing depths differed by less than 5% (ASTM D7400/D7400M-19 2019).

Various authors (e.g. Goto et al. 1992; Nishi et al. 1989) confirmed that microstructure reinforces the bonds between soil particles, leading to an increased V_S and small-strain stiffness shear modulus G_0 compared to unstructured soils. Eslaamizaad and Robertson (1996) and Schnaid (2009) suggested linking G_0/q_t and Q_{tn} to identify the soil microstructure by means of *SCPTu*. The increase in G_0 due to microstructure development is more pronounced than the increase in tip resistance (q_t, Q_{tn}) since the latter is significantly affected by destructuration, i.e. the loss of microstructure during penetration (Robertson 2016). This is also confirmed by numerical analyses of cone penetration in fine-grained structured soils (Hauser and Schweiger 2021). Robertson (2009) introduced the modified normalized small-strain rigidity index K^*_G, determined according to Eq. (4):

$$K^*_G = \left(\frac{G_0}{q_n}\right) \cdot \left(Q_{tn}\right)^{0.75} \tag{4}$$

where q_n ($=q_t-\sigma_v$) defines the net tip resistance. Soils characterized by $K^*_G < 330$ are classified as ideal soils with no or little microstructure, whereby young unstructured soils tend to $K^*_G \approx 100$. Soils with $K^*_G > 330$ are structured according to Robertson (2016).

Soil sampling

Soil sampling was performed at the test sites *Rhesi* and *Lokalbahn Salzburg* based on core drillings, using a single core system without water flushing. *PVC* tubes with a length of 600 mm (*Lokalbahn Salzburg*) and 400 mm (*Rhesi*) were pushed into the soil, retrieved and sealed at both ends with paraffin. Tubes with an outer diameter of 100 mm or 125 mm and a wall thickness of 3.5 mm were used. Offshore sampling at the test site *water reservoir Raggal* was executed using the *CPT*-Ranger system (height = 50 cm, diameter = 7 cm) (Geomil equipment 2021). Foam-lined wooden boxes were used to reduce sample disturbance during transport to the laboratory.

Laboratory testing

V_S was further determined by means of bender element testing (Arroyo 2001). Here, parallel-type bender elements (length = 12 mm, width = 12 mm, thickness = 1.2 mm) with polyurethane coating were used within a triaxial device (Arroyo et al. 2010). Soil specimens with a diameter of 100 mm and a height ranging from 180 to 200 mm were investigated. A sine wave (amplitude = 12 V) with frequencies ranging between 1 to 15 kHz was considered for arrival time detection. V_S is calculated according to Eq. (5) based on the tip-to-tip travel length L_{tt} (between the emitting and receiving bender elements) and the travel time t of the shear wave.

$$V_S = \frac{L_{tt}}{t} \tag{5}$$

No standardized procedures are yet available for defining the arrival time of shear waves (e.g. Arroyo et al. 2010; Lee and Santamarina 2005; Wang et al. 2017). Many authors recommend using the *first reversal* or the *zero after the first reversal* as shear wave arrival time (Arroyo et al. 2010; Lee and Santamarina 2005). Here, the *zero after the first reversal* was used to calculate the arrival time.

V_S of the (presumably) structured material, measured in situ by means of *SDMT* ($V_{S,\mathrm{SDMT}}$), and in the corresponding unstructured material, determined through bender element testing ($V_{S,\mathrm{BE}}$) on reconstituted samples, is compared to quantify the degree of microstructure. Recovered soil specimens are not used for the comparison with reconstituted specimens, since the in situ structure was slightly reduced during sampling. While for unstructured soils $V_{S,\mathrm{BE}}/V_{S,\mathrm{SDMT}} \approx 1$ is expected, smaller ratios are obtained in structured soils (Fonseca and Pineda 2017). Soil specimens considered for bender element testing were oven-dried at 60 °C in the first step. Subsequently, the dried material was mixed with distilled water to reproduce the in situ water content (ranging between 75 and 90% of the liquid limit). The soil–fluid mixture was smeared into cylindrical shells (diameter = 100 mm, height = 220 mm), while ensuring a degree of saturation $S_r > 98\%$, and preloaded vertically ($\sigma'_{\mathrm{v,applied}} = \sigma'_{\mathrm{v,in\ situ}} - 20$ kN/m^2) without lateral deformation. After preloading, soil specimens (height ranged between 170 to 190 mm, diameter = 100 mm) were installed into a triaxial device and a K_0 consolidation procedure was defined to reach the in situ stress state. The in situ stress state was estimated based on the unit weight (determined in the laboratory) and the friction angle (assumed based on experience). Subsequently, V_S (propagated vertically through the soil specimen) was measured by means of bender elements. Due to the fine-grained nature of the investigated (pelitic) sediments, any potential effect of the soil's anisotropy on V_S data is negligible, which ensures direct comparison of the field and laboratory data.

The mineralogy of the soil samples was determined through quantitative X-ray diffraction (*XRD*) analyses (Moore and Reynolds 1997) using a PANalytical X'Pert PRO diffractometer (Co-Kα radiation source) operated at

40 kV and 40 mA and outfitted with a high-speed Scientific X'Celerator detector. The soil powders were prepared by the top-loading technique (Baldermann et al. 2021) and examined in the range of 4–85° 2θ with a step size of 0.008° 2θ and a scan speed of 40 s per step. For data interpretation, the PANalytical X'Pert Highscore Plus software and the ICSD database were applied with an analytical error of < 3 wt%.

The major element composition of the soils was determined by a PANalytical PW2404 wavelength dispersive X-ray fluorescence (*XRF*) spectrometer using standard glass tablets that were prepared in a fully automatic PANalytical Perl'X 3 bead preparation system. Gravimetric analyses of powdered samples (2 g heated to 1050 °C for 1 h) were used to determine the loss on ignition (*LOI*) (Baldermann et al. 2020a). The chemical index of alteration (*CIA*) was calculated based on the *XRF* results, which presents a widely accepted chemical weathering indicator (Bahlburg and Dobrzinski 2011; Goldberg and Humayun 2010; Nesbitt and Young 1982).

The soil (micro)fabric was studied on representative, sampled soil specimens that were cut perpendicular to the bedding plane using scanning electron microscopy (*SEM*). Secondary electron images provide information about the particle shape, size and pore system, while energy-dispersive X-ray spectroscopy (*EDX*) data were collected to chemically fingerprint distinct mineral phases. For further information, reference is made to Collins (1983). Here, Zeiss Sigma 300 VP and Zeiss DSM 982 Gemini microscopes were used for microstructure characterization, which are available at the ZFE and University of Graz, respectively.

The total organic carbon (TOC) and the soil organic matter (SOM) contents were used to describe the influence of biological activity on soil structure formation. Powdered samples were catalytically combusted and the liberated carbon dioxide CO_2 analysed by a non-dispersive infrared detector using a Shimadzu TOC-VcPH + ASI-V analyser with an analytical error of ± 5% (Baldermann et al. 2020a). The *SOM* content was calculated based on *TOC* values by assuming a conversion factor of 2.1 (i.e. $SOM = TOC \cdot 2.1$).

The pore water of the soil specimens was characterized with respect to the electric conductivity (*EC*), *pH* value and elemental concentration. *EC* was determined based on a WTW LF 330 m multimeter connected to a TetraCon 325 probe. A WTW pH 330 m multimeter in combination with a WTW SenTix41 probe was used to analyse *pH*. The *pH* electrode was calibrated against NIST buffer standard solutions at $pH = 7$ and $pH = 10$ at 23 °C (Steindl et al. 2019) with an analytical precision of ± 0.03 pH units. Major, minor and trace element analyses were performed on a Perkin Elmer Optima 8300 DV inductively coupled plasma optical emission spectrometer (ICP-OES) on acidified sample aliquots as well as via ion chromatography (Dionex ICS-3000) and automated titration (Schott TA20plus titrator) at an analytical precision of < 5% (determined via NIST 1640a, in-house and SPS-SW2 Batch 130 standards). The saturation index *SI*, defined according to Eq. (6), was used to determine whether a mineral is saturated ($SI = 0$), undersaturated ($SI < 0$), or supersaturated ($SI > 0$) with respect to the pore water:

$$\mathrm{SI} = \log \frac{\mathrm{IAP}}{K_{sp}} \tag{6}$$

where *IAP* and K_{sp} represent the ion activation product and the mineral-specific solubility constant (e.g. quartz, calcite and mica), respectively.

The age of the investigated soils was determined by radiocarbon dating (*C-14*) of organic components present in the soils (e.g. wood sticks or plant remnants), with recognition of the published radiocarbon decay constant (Garrett 1963). All measurements were executed at the Poznań Radiocarbon Laboratory using accelerator mass spectrometry (*AMS*).

Results and discussion

Soil classification

Lokalbahn Salzburg

The test site *Lokalbahn Salzburg* is located in Salzburg city (47° 48′ 58.8492" N/13° 2′ 42.2592″ E) and in situ testing (*CPTu, SDMT*) as well as soil sampling was executed down to a depth equal to 25 m. The subsurface sediments can be divided into three main lithologies based on *CPTu* measurements, denoted *CPTu 8/20 and CPTu 19/20* in the following, i.e. *L1—sandy gravel*, *L2—sand-silt alternations* and *L3—silty clay*. The groundwater table was situated 1.5 m below ground level during test execution. *L1* is characterized by a thickness of 4 m and the measured q_c (5 to 20 MPa) and f_s (20 to 160 kPa) values show a large scatter, indicating a heterogeneous composition (Fig. 1a, b). Small R_f (< 1%) and u_2 values (Fig. 1c) imply drained material behaviour during in situ testing. These sediments are classified as (6) sands (clean sand to silty sand) according to Robertson (2009) (blue symbols in Fig. 2a) and silty gravel with sand (GM) based on ASTM D2487-17e1 2017 (USCS). *Sand-silt alternations (L2)* are situated between 4 to 9 m below ground level and exhibit reduced q_c and f_s values compared to *L1*, ranging from 0.8 to 4.0 MPa and 10 to 80 kPa, respectively. The erratic patterns of u_2 is consistent with varying soil behaviour types (red symbols in Fig. 2a: (3) clays to (5) sand mixtures). Although the *PSD* varies within *L2* (fines-fraction varies between 19.2% and 97.4%), silt and sand remain the dominant fractions according to ISO 14688-1 (2017) (Fig. 3a: *cl' sa Si* to *si Sa*). The homogeneous section *L3*

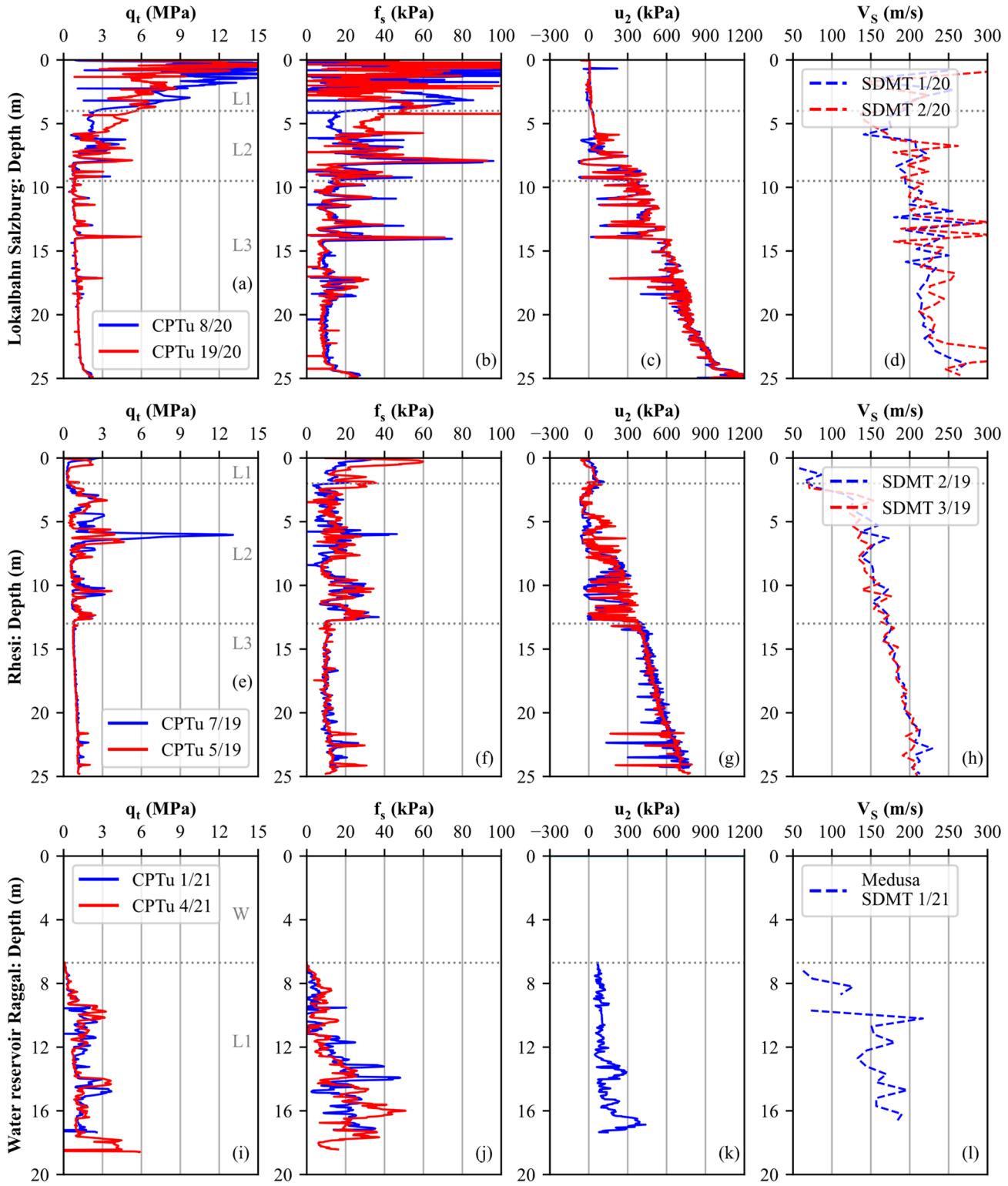

Fig. 1 Compilation of *CPTu* and *DPDH* measurements (q_t, f_s, u_2, V_S) at test sites *Lokalbahn Salzburg* (top row), *Rhesi* (middle row) and *water reservoir Raggal* (bottom row)

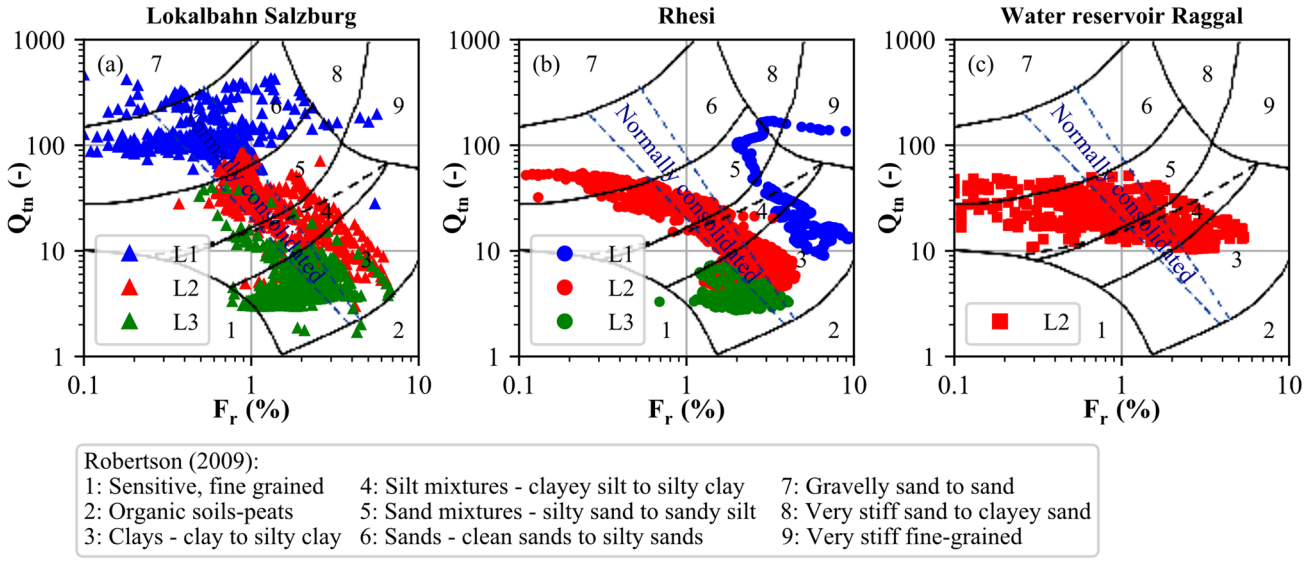

Fig. 2 Soil classification according to Robertson (2016) for test sites **a** *Lokalbahn Salzburg*, **b** *Rhesi* and **c** *water reservoir Raggal*

is characterized by reduced q_c (< 2 MPa) and f_s (< 15 kPa) values, high excess pore water pressures at position u_2 and V_S values ranging from 200 to 300 m/s (Fig. 1a–d). These sediments are classified as (3) clays according to Robertson (2009) (green symbols in Fig. 2a), sandy clayey silts (*sa' cl Si*) according to ISO 14688-1 and lean clays (*CL*) according to USCS (ASTM D2487-17e1). The Atterberg limits show a small scatter ($PL = 19.5$ to 23.6%, $LL = 39.7$ to 42.2%; Fig. 3b), and all investigated specimens are classified as medium plasticity clays based on the Casagrande chart. As shown in Fig. 3b–d, w_{nat}, ρ_d, ρ_{sat} and ρ_s vary from 25.3 to 37.7%, 1.41 to 1.65 g/cm^3, 1.94 to 2.09 g/cm^3 and 2.77 to 2.78 g/cm^3, respectively. The *SOM* contents vary between 0.3 and 0.9%, but show no significant trend over depth. The soil age was investigated at two depths (− 12 m and − 20 m). It is evident that the sediments were deposited in the Pleistocene, at 32,400 ± 500 and 36,100 ± 700 years before present (*BP*).

Rhesi

The test site *Rhesi* is situated in the western part of Austria about 2 km south of Lake Constance (47° 28′ 38.4924″ N/9° 40′ 5.4912″ E). All investigations were executed within a rectangular area of approximately 75 × 25 m down to a depth of 25 m below ground level. The subsurface at the test site *Rhesi* can be divided into three lithologies: *L1—silty sand*, *L2—sand-silt alternations* and *L3—silty clay* (see Fig. 1e–h). *L1* represents a 2 m thick top layer that is characterized by a large heterogeneity, leading to a strong variation of *CPTu* measurements (Fig. 1) and *SBTn* classifications (blue symbols in Fig. 2b). The groundwater table was situated 0.8 m below ground level during test execution. While q_c and f_s are smaller than 1 MPa and 10 kPa in fine-grained sections of lithology *L2*, they can increase up to 5 MPa and 30 kPa in coarser sections. The reverse trend is observed for u_2 measurements. Since R_f varies between 1 and 3%, the data yield a wide scatter within the *SBTn* chart of Robertson (2009), ranging from (3) clay to (6) sand (red symbols in Fig. 2b) and generally indicating normally consolidated conditions (Robertson 2009). These sediments present a fines-content ranging from 33 to 92% and are classified as lean clays (CL) to silty, clayey sands (SC-SM) based on USCS (ASTM D2487-17e1). All data are situated above the A-line within the Casagrande chart, even though the particle size distribution is characterized by a pronounced scatter (ranging from *sa' cl Si* to *cl' si Sa* according to ISO 14688-1, Fig. 3e). The sediments of *L3* (Fig. 1: $q_c < 1$ MPa, $f_s \approx 10$ to 15 kPa and $R_f = 1$ to 1.5%) are characterized as (3) clays according to Robertson (2009) (green symbols in Fig. 2b), present a fines-content larger than 91% (lean clays *CL* to fat clays *CH* according to USCS; *sa' cl Si* to *sa' Cl/Si* according to ISO 14688-1) and show a slight increase of *LL* and *PL* over depth (triangles in Fig. 3f). The values for w_{nat}, ρ_d, ρ_{sat} and ρ_s vary from 34 to 38% (Fig. 3f), 1.28 to 1.38 g/cm^3 (Fig. 3g), 1.8 to 1.86 g/cm^3 (Fig. 3g) and 2.64 to 2.69 g/cm^3 (Fig. 3h), respectively, within *L3*. The *SOM* contents vary over depth and present the highest values within *L3* (0.4 to 1.1%). Age dating of sediments collected at − 3 m and − 17 m depth indicates that sediment deposition occurred in the Holocene, between 3,800 and 4400 ± 40 years BP.

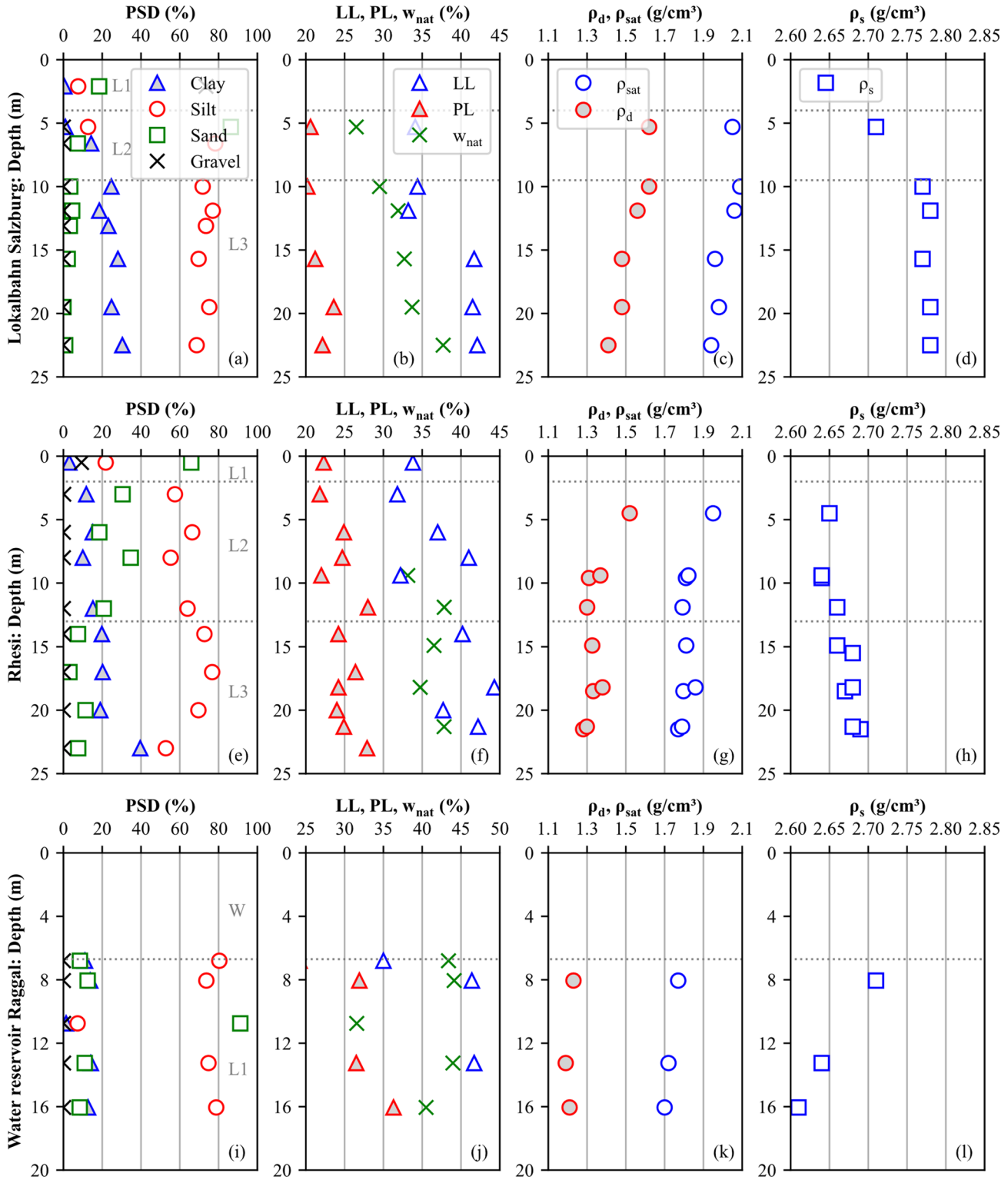

Fig. 3 Compilation of results from geotechnical laboratory testing (particle size distribution *PSD*, liquid limit *LL*, plastic limit *PL*, dry density ρ_d, saturated density ρ_{sat}, particle density ρ_s) at test sites *Lokalbahn Salzburg* (top row), *Rhesi* (middle row) and *water reservoir Raggal* (bottom row)

Water reservoir Raggal

The test site *water reservoir Raggal*, located in the western part of Austria (47° 13′ 13.2024″ N/9° 50′ 38.0724″ E), is operated by the energy supplier *illwerke vkw* and is part of the hydropower plant *Oberstufe Lutz* (Oberhollenzer et al. 2022b). Due to natural sedimentation, about 50,000 m^3 of material is deposited within the reservoir every year. In situ testing and soil sampling were executed from a floating pontoon using a modular stand-alone system (Fox-150) by Geomil equipment (2022) as pushing device. The water depth amounted to approximately 7 m during test execution. The sediments were investigated down to approximately 15 m below seabed. The sedimentation history within the *water reservoir Raggal* is reflected in the form of alternating fine- and coarse-grained layers. The sand-silt alternations are characterized by an erratic distribution of *CPTu* patterns over depth (*L1* in Fig. 1i–k). Values for q_c and f_s vary from 0.7 to 3.5 MPa and 5 to 50 kPa, respectively. V_S varies between 50 and 230 m/s over depth and presents increased values within sand-dominated sections (Fig. 1l). These young deposits, characterized by an age of < 50 years, are mainly defined as (4) silt and (5) sand mixtures based on Robertson (2009) (red symbols in Fig. 2c). The *PSDs* of soil specimens reveal that an increased sand content (e.g. at − 10.5 m) correlates with higher q_t and lower u_2 values (Figs. 1i, 3i). Four soil samples, classified as clayey, sandy silts (*cl' sa' Si*) according to ISO 14688-1, were recovered within fine-grained sections. These specimens present a fines-content of > 90% and are classified as organic silts (OL, OH) based on the USCS. Due to their high *SOM* contents, ranging between 0.63 and 2.1%, all data are situated below the A-line within the Casagrande chart. Small ρ_d from 1.19 to 1.23 g/cm^3 and ρ_{sat} from 1.74 to 1.77 g/cm^3 and a high w_{nat} of > 40% were determined within fine-grained layers (Fig. 3). The ρ_s slightly decreases from 2.71 to 2.61 g/cm^3 over depth (Fig. 3l).

Seismic in situ testing

SBTn charts according to Robertson (2016) are shown for all three test sites in Fig. 4. The results obtained for test site *Lokalbahn Salzburg* are situated at the transition between unstructured and structured soils (Fig. 4a). While most samples from *L1* (sand gravel) and *L2* (sand-silt alternations) fall within $K^*_G > 330$, the samples from *L3* (pelitic sediments) are characterized by slightly smaller K^*_G values ($K^*_G \approx 330$, on average). However, individual K^*_G values of *L3* are significantly larger than 330 (Fig. 4a). These results are in good agreement with previous investigations executed at construction sites in Salzburg city (Oberhollenzer et al. 2019).

SBTn results are situated at the transition between ideal (unstructured) and structured soils for test site *Rhesi* (Fig. 4b). In contrast to the previous test site, the top layer (*L1*) and sand-silt alternations (*L2*) are characterized by $K^*_G < 330$. Since *L3* (clayey silt) shows a bit higher K^*_G values, soil microstructure slightly increases over depth according to Robertson (2016). However, K^*_G remains smaller than 330 within *L3*. Fine-grained deposits investigated at test site *water reservoir Raggal* are again situated at the transition between structured and unstructured soils (Fig. 4c). While sand-dominated layers are characterized by $K^*_G > 330$ (see 4 data points situated on the right side of the $K^*_G = 330$ line in Fig. 4c), K^*_G values smaller than 330 are observed in silt-dominated sections.

Since the microstructure of pelitic sediments is investigated in detail, the in situ data were filtered based on the *SBTn* to enable a comparison of fine-grained layers investigated at the different test sites. Sediments characterized by *SBTn* = 3 (*Lokalbahn Salzburg, Rhesi*) and *SBTn* = 4 (*water reservoir*

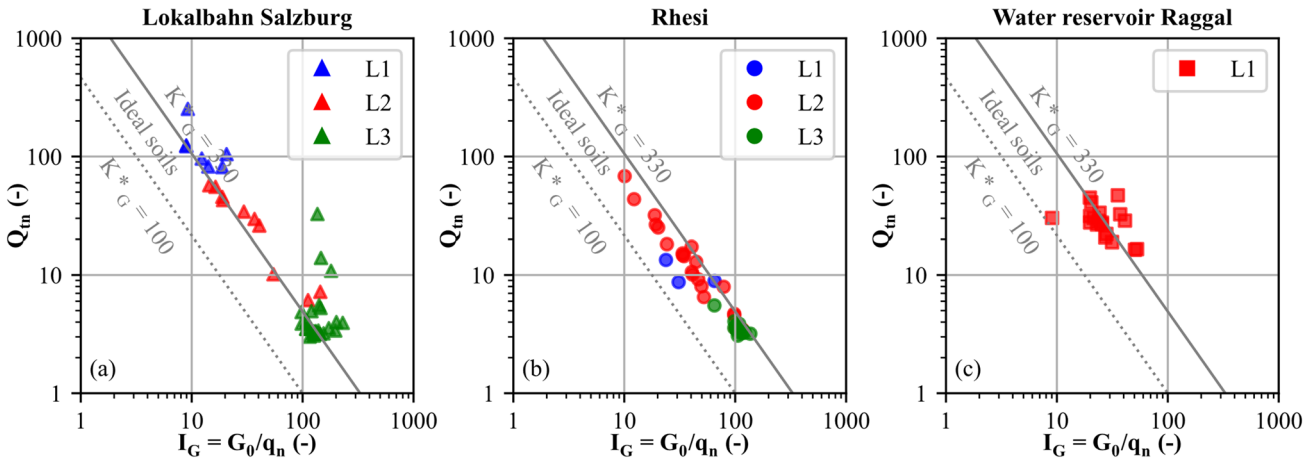

Fig. 4 Detection of microstructure at test sites **a** *Lokalbahn Salzburg*, **b** *Rhesi* and **c** *water reservoir Raggal* according to Robertson (2016)

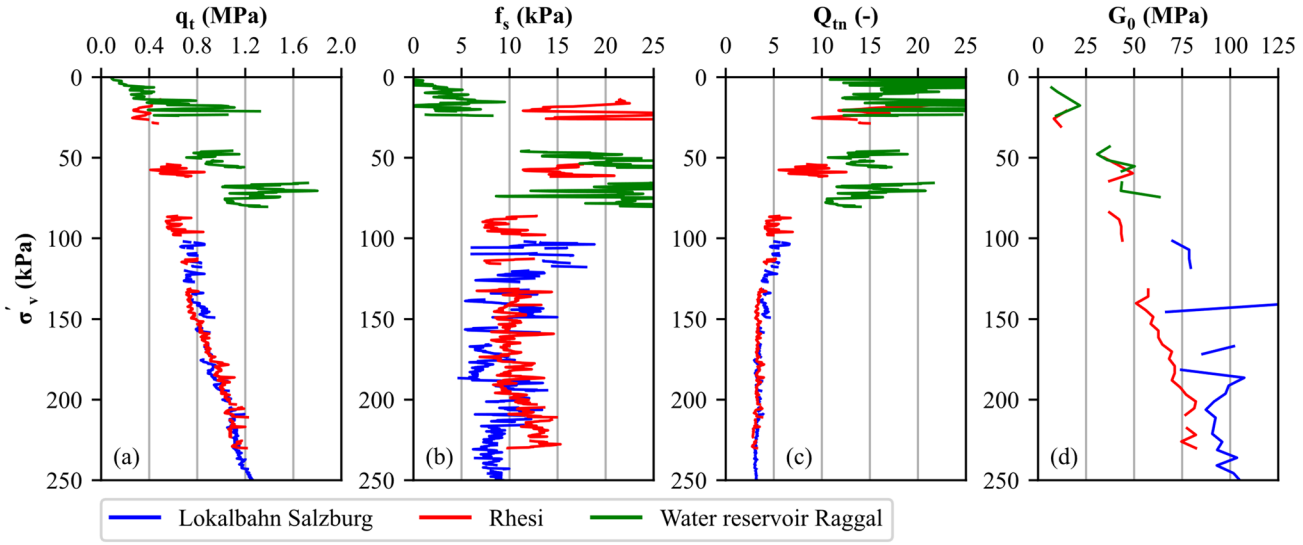

Fig. 5 Comparison of the corrected tip resistance q_t, sleeve friction f_s, updated normalized tip resistance Q_{tn} and small-strain stiffness shear modulus G_0 for test sites *Lokalbahn Salzburg*, *Rhesi* and *water reservoir Raggal*

Raggal) are used for further discussion. The filtered q_t, f_s, Q_{tn} and G_0 values are plotted against σ'_v for a direct comparison in Fig. 5. It is shown that q_t and f_s are in good agreement between test sites *Lokalbahn Salzburg* and *Rhesi*, especially in greater depths. While the increase in q_t with depth correlates with higher effective stresses, f_s seems to be less sensitive to changes in stress level, and Q_{tn} remains approximately constant (due to the normalization). However, G_0 is higher at test site *Lokalbahn Salzburg,* which is related to the higher density (Fig. 3c). While *CPTu* and *SDMT* were executed to a final depth of 25 m at both locations, *CPTu* measurements for test site *water reservoir Raggal* are only available for σ'_v smaller than 75 kPa, making a direct comparison with the other sites difficult. The slightly smaller clay content and higher sand content lead to an increase of q_t and Q_{tn} compared to test sites *Lokalbahn Salzburg* and *Rhesi* (Fig. 5a, c). G_0 results increase over depth and are in good agreement with the two other locations (Fig. 5d).

K^*_G results, calculated based on the filtered Q_{tn} and G_0 values, are shown in Fig. 6 using box plots. While the oldest sediments, investigated at the test site *Lokalbahn Salzburg* (age: 32,400—36,100 years BP), lead to the highest K^*_G, the smallest K^*_G is obtained within the *water reservoir Raggal* (age: < 50 years). However, the differences in K^*_G are small between the three locations, and all results are situated close to the proposed transition between ideal and structured soils ($K^*_G = 330$).

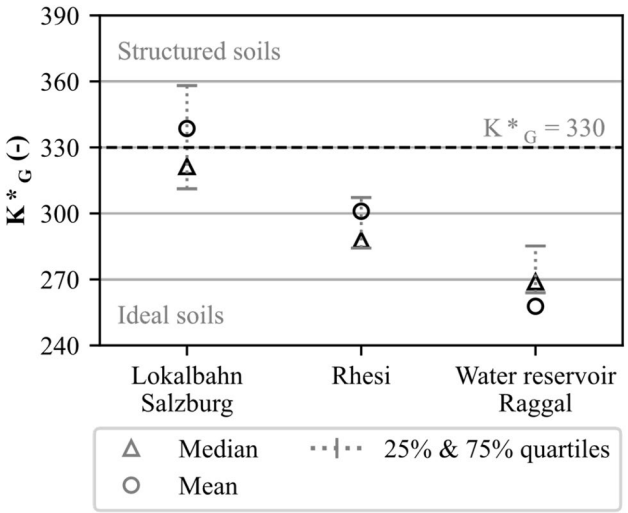

Fig. 6 Comparison of the modified normalized small-strain stiffness rigidity index K^*_G for test sites *Lokalbahn Salzburg*, *Rhesi* and *water reservoir Raggal* by means of box plots

Comparison of in situ and reconstituted shear wave velocity

The V_S data obtained from bender element testing and *SDMT* are shown in Fig. 7 (top row) for the three test sites. Additionally, the $V_{S,BE}/V_{S,SDMT}$ ratios are presented in the bottom row of Fig. 7. It can be observed for the test sites *Lokalbahn Salzburg* and *Rhesi* that the bender element results are smaller compared to the in situ measurements, which leads to $V_{S,BE}/V_{S,SDMT}$ ratios smaller than 1, indicating the presence of a microstructure. Although the ratios are

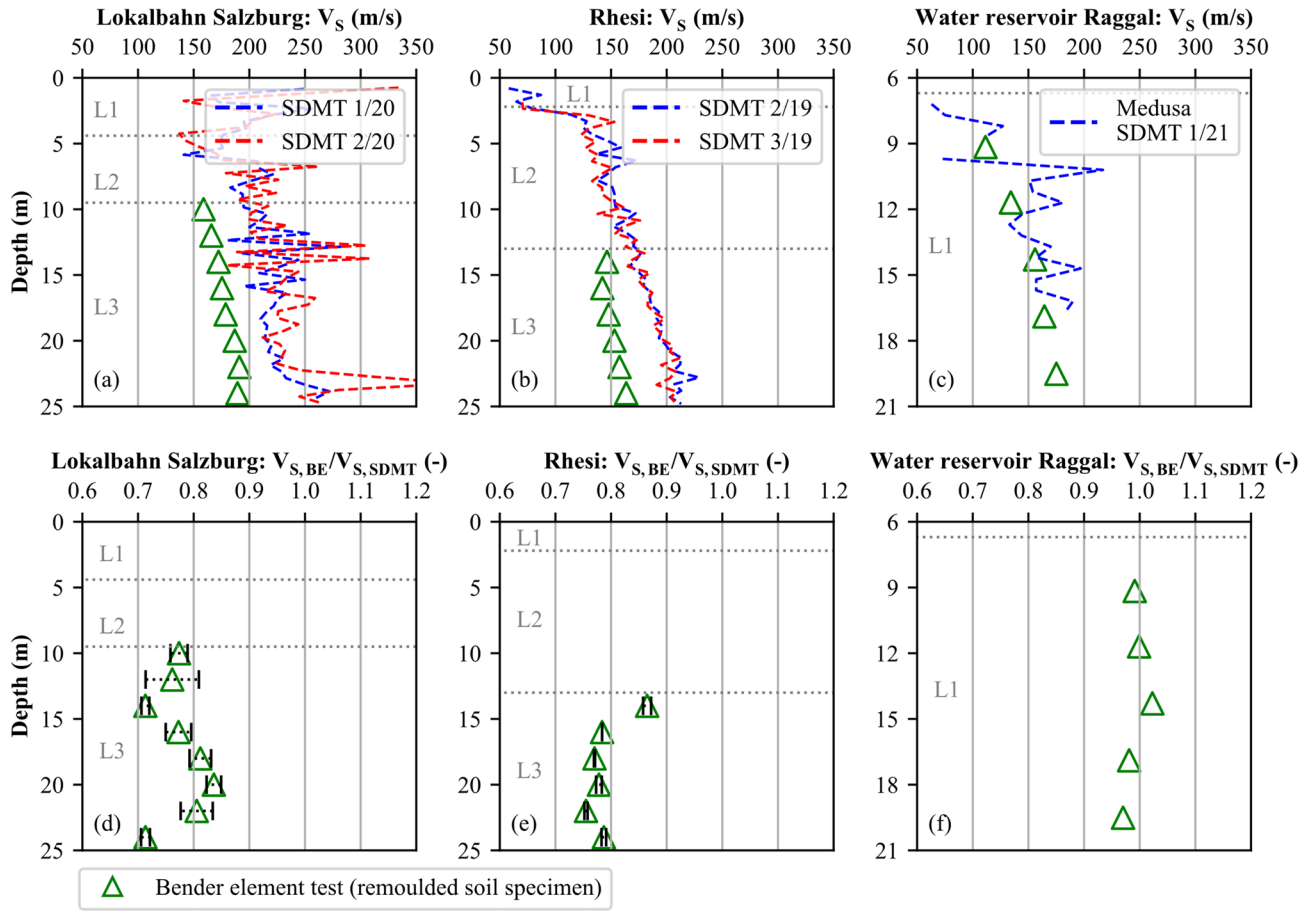

Fig. 7 Comparison of in situ and reconstituted shear wave velocities ($V_{S,SDMT}$, $V_{S,BE}$) for test sites *Lokalbahn Salzburg* (left column), *Rhesi* (middle column) and *water reservoir Raggal* (right column). While white triangles are determined based on averaged *SDMT* readings, the scatter in $V_{S,BE}/V_{S,SDMT}$ is indicated by dotted horizontal lines

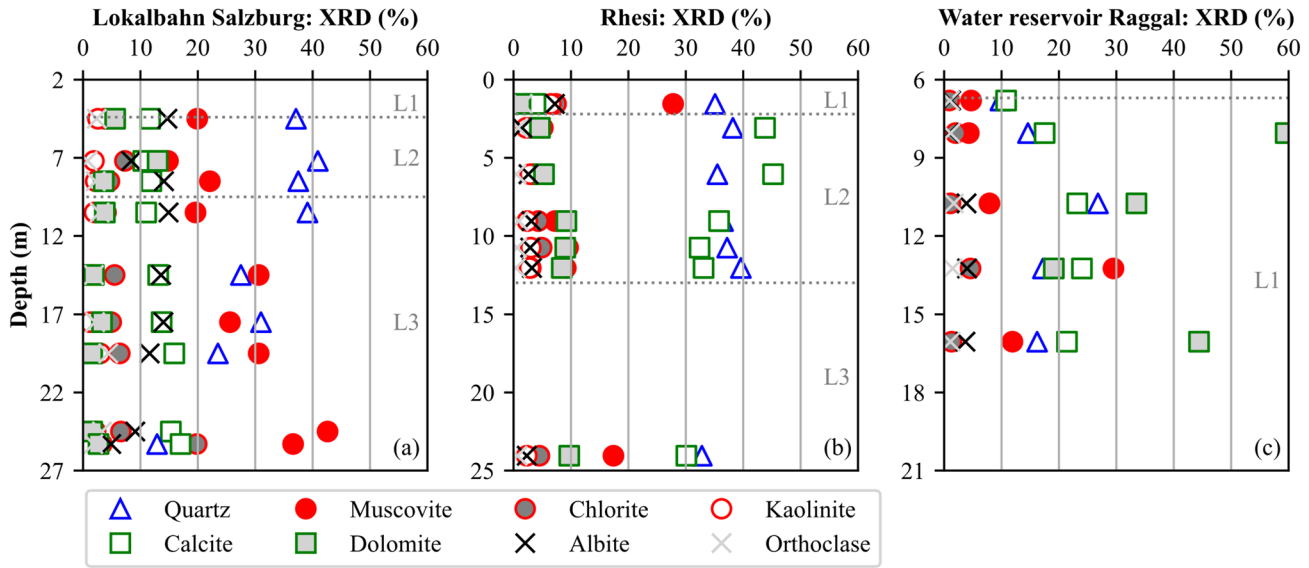

Fig. 8 Compilation of X-ray diffraction (*XRD*) data for test sites **a** *Lokalbahn Salzburg*, **b** *Rhesi* and **c** *water reservoir Raggal*

characterized by some scatter, a value of approximately 0.8 is reached at both test sites, which does not change significantly over depth ($V_{S,BE}/V_{S,SDMT} \approx 0.7–0.9$; Fig. 7d and e). At the test site *water reservoir Raggal*, $V_{S,BE}/V_{S,SDMT}$ ratios of approximately 1 are observed, indicating little if any microstructure within the young deposits (Fig. 8f). Consequently, the presence of soil structure is indicated at 2 out of 3 test sites based on the obtained $V_{S,BE}/V_{S,SDMT}$ ratios. In the following, possible explanations for microstructure formation are discussed based on mineralogical, hydrochemical and microstructural laboratory testing.

Mineralogical and chemical characterization of soils

The mineralogy at test sites *Lokalbahn Salzburg*, *Rhesi* and *water reservoir Raggal* is mainly composed of quartz, clay minerals, carbonates (calcite and dolomite) and feldspar (K-feldspar and albite), which differ in quantity between the locations and along vertical profiles. At test site *Lokalbahn Salzburg* (Fig. 8a), the amount of quartz decreases from 40.4% to 16.2% over depth, while clay minerals present the inverse trend. The latter group is mainly composed of muscovite (19.9–42.6%) and, to a smaller extent, chlorite (3.7–6.6%) and kaolinite (1.2–3.0%). Both, calcite and albite amount to approximately 13% and show no significant changes over depth. The mineralogical composition at test site *Rhesi* (Fig. 8b) is dominated by quartz (32.8–39.6%), calcite (3.8–45.2%), dolomite (1.2–9.7%) and muscovite (3.3–27.8%). The reduced carbonate content and the high amount of clay minerals within *L1* are strong indicators of a different depositional history compared to *L2* and *L3*. This observation agrees with recordings proving that the river *Dornbirner Ach* (draining limestone and marl lithologies) dominated the early sedimentation at this test site. Later, the *Alpine Rhine* was artificially diverted to its present river bed. *L2* and *L3* consist of quartz (32.8–39.6%), muscovite (3.3–17.4%), calcite (30.1–45.2%) and dolomite (4.6–9.7%). Accordingly, test site *Rhesi* is characterized by higher calcite and lower muscovite contents within *L2* and *L3* compared to *Lokalbahn Salzburg*. The mineralogy at test site *water reservoir Raggal* presents a strong scatter over depth, even though quartz (9.8–26.8%), muscovite (4.3–29.5%), chlorite (0.9–4.6%), calcite (10.8–24.0%), dolomite (19.1–71.7%), albite (0.9–4.0%) and orthoclase (1.0–1.7%) dominate (Fig. 8c).

The *CIA* values indicate a high to very high degree of weathering, ranging between 76 and 89 at test sites *Lokalbahn Salzburg* and *Rhesi*, which is typical for postglacial deposits. The younger sediments at test site *water reservoir Raggal* show lower *CIA* values ranging between 67 and 74, suggesting that physical particle breakdown is more efficient than chemical weathering (Nesbitt and Young 1982). It was observed at each test site that the *CIA* values slightly increase over depth since deeper situated layers are exposed to interactions with groundwater and, thus, chemical weathering for a longer period of time.

Pore water chemistry

The *pH* values range between 7.4 and 8.2 at all locations, indicating a slightly alkaline environment. The *EC* values range between 462 and 1430 µS/cm, yielding increased values within the pelitic sections. Therefore, *L3* at test sites *Lokalbahn Salzburg* and *Rhesi* shows the highest *EC* values along their respective profiles, but the fine-grained layers at test site *water reservoir Raggal* exhibited the highest *EC* values along all test sites ($EC = 1430$ µS/cm).

The concentrations of Ca^{2+}, Mg^{2+}, K^{+}, Na^{+}, Cl^{-}, NH_4^{+} and SO_4^{2-} ions within the pore water remain below 160 mg/l within the postglacial deposits. Higher amounts of HCO_3^{-} ions can be related to the dissolution of carbonate minerals and natural gas occurrences at test site *Lokalbahn Salzburg* (163 to 348 mg/l) and *Rhesi* (237 to 381 mg/l), respectively. The concentrations of Ca^{2+} (167–364 mg/l), SO_4^{2-} (142–232 mg/l) and HCO_3^{-} (438 to 1086 mg/l) ions vary strongly at test site *water reservoir Raggal*. The *SI* values of quartz, aragonite, calcite and albite were calculated from pore water concentration data and are shown in Fig. 9. Near surface layers at test site *Lokalbahn Salzburg* are characterized by $SI \approx 0$ for all minerals of interest (Fig. 9a). In contrast, undersaturation ($SI < 0$) is indicated for aragonite, calcite and albite within *L3*. Test sites *Rhesi* and *water reservoir Raggal* indicate an oversaturation ($SI > 0$) with respect to calcite and aragonite in all pore waters (Fig. 9b), suggesting an authigenic formation of these carbonate minerals. While calcite cement formation can be reasonably considered to have a stabilizing effect on soil structure, silicate weathering (indicated by a negative SI_{Albite}) leads to the reverse trend, as recently documented by artificial soil cementation experiments (Oberhollenzer et al. 2022a). Since silicate weathering needs more time compared to calcite formation, a stabilizing effect and related microstructure formation is expected at test sites *Rhesi* and *water reservoir Raggal*.

Microstructural characterization

The soil fabric of undisturbed pelitic specimens recovered at −25.3 m, −22.2 m and −15.8 m at test sites *Lokalbahn Salzburg*, *Rhesi* and *water reservoir Raggal* is shown in Fig. 10. The presence of lamination is indicated by red shadings for each test site (Fig. 10a, b and c). Since individual soil specimens were rotated for analysis, the red dashed lines are disposed to the horizontal. It is evident that particle sizes differ between the three test sites. While soil specimens recovered at test sites *Lokalbahn Salzburg* and *Rhesi* are in

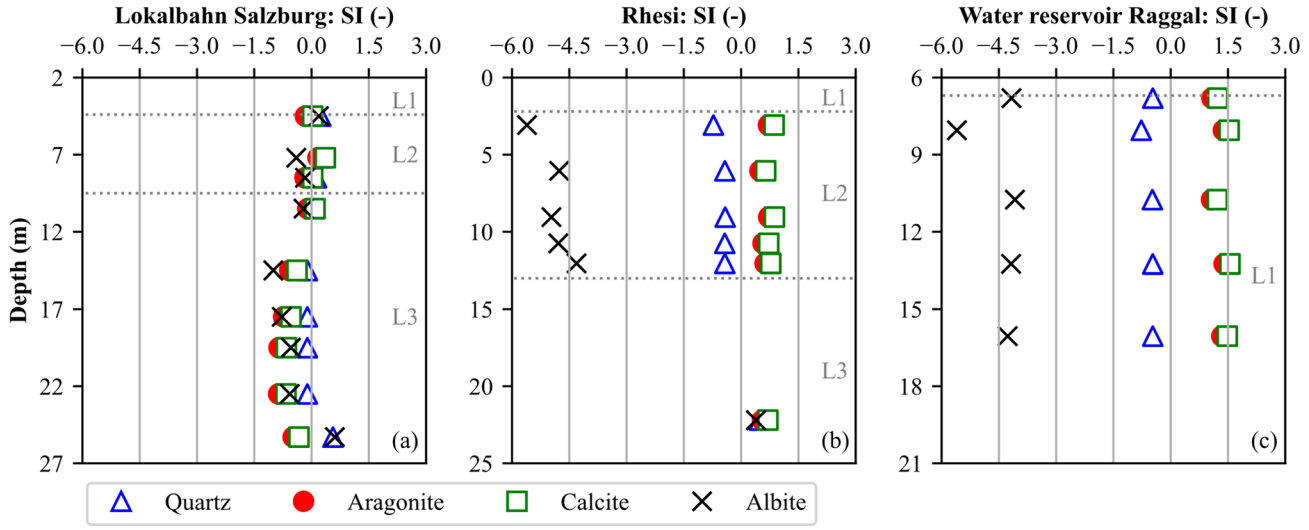

Fig. 9 Saturation indices (*SI*) calculated for several mineral phases at test sites **a** *Lokalbahn Salzburg*, **b** *Rhesi* and **c** *water reservoir Raggal*

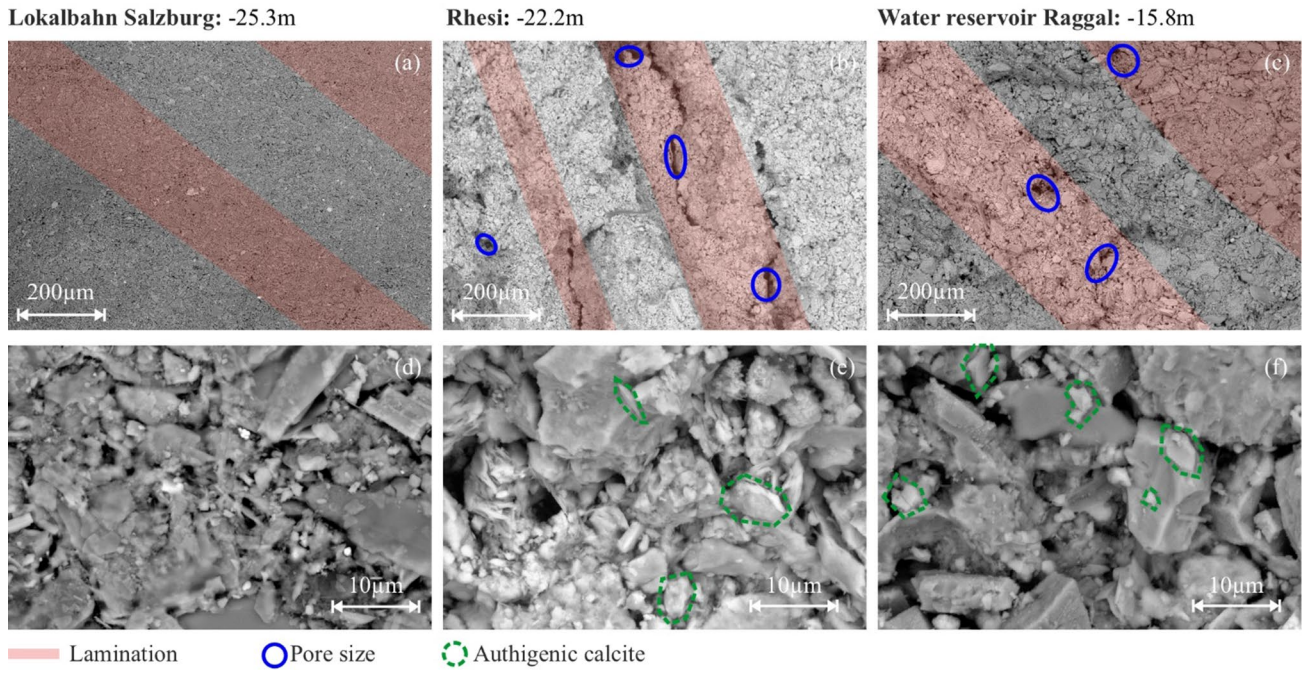

Fig. 10 *SEM* images showing fabric and microstructural features of sampled soils from test sites *Lokalbahn Salzburg* (left column), *Rhesi* (middle column) and *water reservoir Raggal* (right column)

good agreement with respect to their *PDS* (*sa' cl Si*), sediments from test site *water reservoir Raggal* indicate a higher sand content (*cl' sa' Si*). The pore systems (indicated by blue, solid ellipses) are aligned along the lamination at test sites *Rhesi* (Fig. 10b) and *water reservoir Raggal* (Fig. 10c). In contrast, no such 'systems', i.e. large voids, are observable at test site *Lokalbahn Salzburg* (Fig. 10a). Since test sites *Lokalbahn Salzburg* and *Rhesi* are characterized by similar particle sizes, differences in fabric can be related to changes in ρ_d and e. Consequently, the open fabric at test site *Rhesi* ($\rho_{sat} = 1.81$ g/cm^3, $e = 1.1$) is characterized by a lower ρ_d and higher e than test site *Lokalbahn Salzburg* ($\rho_{sat} = 1.95$ g/cm^3, $e = 0.9$). The change in ρ_d is caused by an open fabric within under-consolidated sediments at test site *water reservoir Raggal* ($\rho_{sat} = 1.74$ g/cm^3, $e = 1.2$). As the oldest and youngest sediments were investigated in Salzburg

and Raggal, respectively, it can be seen that soil density (ρ_d, ρ_{sat}) increases, while w_{nat} and e decrease with sediment age (Fig. 3).

Calcite ($CaCO_3$), characterized by rhomb-shaped crystals at test site *Rhesi* (green, dashed polylines in Fig. 10), is likely of authigenic origin, corroborating the pore water chemical data. The calcite cements grow within the pore system and present a pore-infill or interconnect other detrital particles, such as quartz, clay minerals, carbonate clasts and feldspar grains, which both stabilizes the sediment's fabric. In contrast, no significant amount of authigenic calcite was recognized at test site *Lokalbahn Salzburg* (Fig. 10d). The sediments investigated at test site *water reservoir Raggal* present an open fabric, which is characterized by pore systems that are only filled by calcite to a small extent. As shown in Fig. 10f, authigenic calcites are mainly formed on top of existing carbonate grains, indicated as epitaxial growth or overgrowth (Baldermann et al. 2020b).

SEM results of reconstituted soil specimens are shown for the test sites *Lokalbahn Salzburg* and *Rhesi* in Fig. 11. The material used for reconstituting the specimens was sampled at − 19.2 m and − 22.2 m, respectively (see Fig. 11). Both specimens do not show lamination and are characterized by a smaller pore space compared to the natural specimens (see Fig. 10). Clay minerals are aligned mostly in parallel (see green indication in Fig. 11) and do not form a card house structure as it is often observed in natural clays. No evidence for the formation of stabilizing (i.e. structure-forming), authigenic calcite cements was found in the reconstituted samples at both sites, all indicating that the fabric differed compared to the sampled specimens.

Discussion

Sediment ageing, which is known to significantly influence the mechanical behaviour of soils (Schmertmann 1991), includes (i) structure-forming processes, such as mineral authigenesis, and (ii) structure-destabilizing processes, such as chemical and physical weathering. These two processes are difficult to separate as they may occur simultaneously over time (Burland 1990; Leroueil and Vaughan 1990; Mitchell 1976). The formation of authigenic calcite cements was recognized at two locations (*Rhesi*, *water reservoir Raggal*) based on a *SEM* study and was confirmed by the soil's pore water chemistry. Micron-sized calcite particles clog formerly open pore spaces and interconnect detrital particles. Accordingly, this cementation process leads to an increased V_S (DeJong et al. 2022; Schnaid 2009), which was confirmed by comparing the V_S values determined in situ and by means of bender element testing on reconstituted soil specimens. The considered postglacial, pelitic

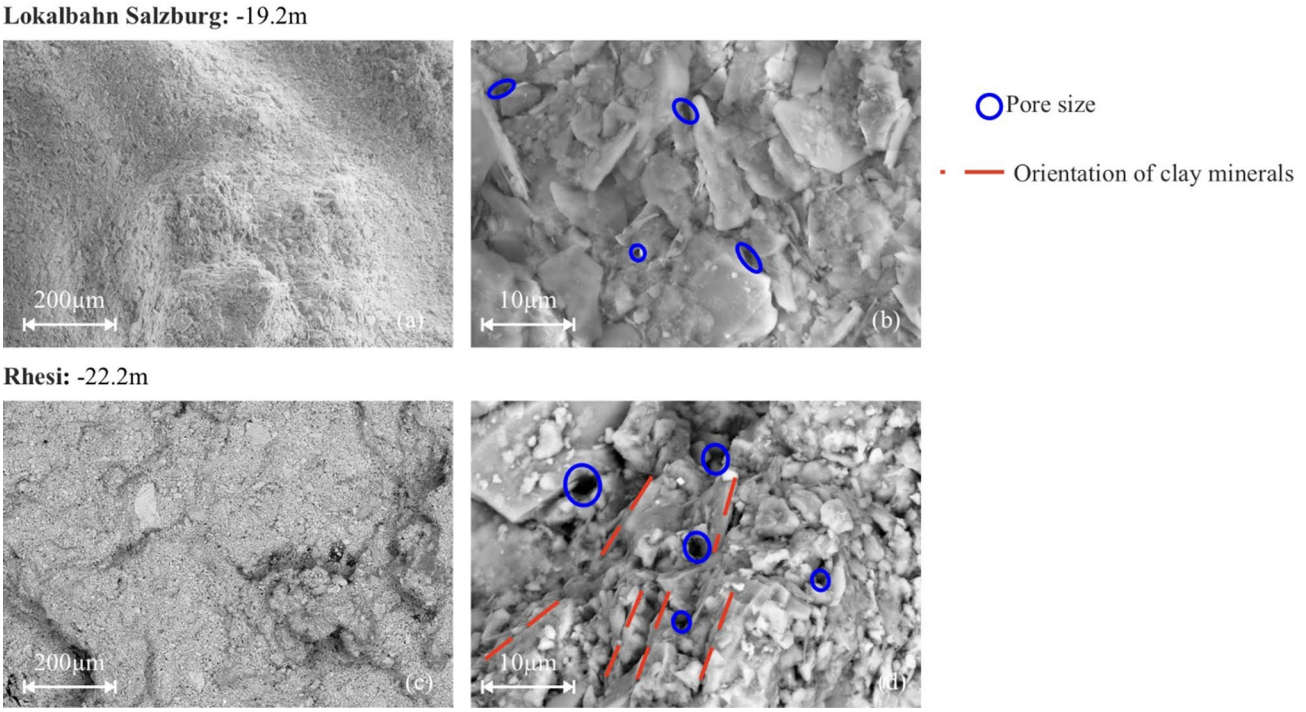

Fig. 11 *SEM* images showing fabric and microstructural features of reconstituted soils from test sites *Lokalbahn Salzburg* (left column) and *Rhesi* (middle column). Note the absence of lamination, the finer pore system and the preferred orientation of clay mineral particles in the reconstituted soils compared to the sampled soil specimens

sediments at the test site *Rhesi* are characterized by $V_{S,BE}/V_{S,SDMT}$ ratios < 1, suggesting the presence of soil structure, which is in good agreement with published seismic *CPTu* results (Oberhollenzer et al. 2019). The influence of soil structure on results of oedometer and triaxial tests was not investigated in this study, as the specimens used for mechanical testing were slightly disturbed. While an interlocking effect due to cementation was observed at test site *Rhesi*, an overgrowth of $CaCO_3$ cements on existing detrital calcite surfaces was observed at test site *water reservoir Raggal*. It is assumed that the latter has only a minor stabilizing effect on soil structure in these extremely young, pelitic soils, since a $V_{S,BE}/V_{S,SDMT}$ ratio of approximately 1 was determined. Since $V_{S,BE}/V_{S,SDMT} < 1$ are characterized by K^*_G larger than 280, it is suggested to slightly adjust the transition proposed by Robertson (2016) (i.e. unstructured soils: $V_{S,BE}/V_{S,SDMT} \approx 1$, $K^*_G < 280$). The results indicate that $V_{S,BE}/V_{S,SDMT}$ ratios are more sensitive to changes in microstructure compared to K^*_G and are therefore preferred. Silicate mineral weathering, which was observed at all three test sites, leads to the opposing effect, i.e. microstructure destabilization. The latter reactions take longer time spans compared to the authigenic formation of $CaCO_3$ cements and, thus, the structure-forming process is assumed to be dominant for the considered postglacial sediments. Different microstructure-forming mechanisms must be considered as driving force at test site *Lokalbahn Salzburg*, since no authigenic formation of $CaCO_3$ is indicated based on *SEM* imaging and pore water chemistry data. Further investigations are required to reveal to what extent additional structure-forming processes and the significantly greater burial age may play a role for the formation of these sediments.

Conclusion

This study investigates the composition and microstructure of lacustrine, fine-grained sediments at three test sites within the Alpine region. While postglacial deposits are studied at the test sites *Lokalbahn Salzburg* and *Rhesi*, significantly younger soils (< 50 years) were investigated within the *water reservoir Raggal*. In situ testing by means of *CPTu* and *SDMT* in combination with soil, as well as pore water sampling to enable geotechnical, mineralogical, hydrochemical and microstructural laboratory testing, were executed at each location. The most important findings can be summarized as follows:

- The modified normalized small-strain rigidity index K^*_G was used to distinguish structured and unstructured soils. K^*_G was found to slightly increase with sediment age and degree of calcite cementation, however, not being very sensitive to changes in microstructure.
- The degree of soil structure was estimated by $V_{S,BE}/V_{S,SDMT}$: $V_{S,BE}/V_{S,SDMT}$ ratios < 1 indicate the presence of soil structure in postglacial deposits, while younger, unstructured deposits yield $V_{S,BE}/V_{S,SDMT}$ of approximately 1.
- If the degree of structure is not evaluated based on $V_{S,BE}/V_{S,SDMT,}$ it is recommended to define the transition between unstructured and structured soils at $K^*_G = 280$ (at least for fine-grained sediments within the Alpine region).
- The test sites *Rhesi* and *water reservoir Raggal* are characterized by the authigenic formation of rhomb-shaped calcite cements, leading to an interparticle bonding, especially at test site *Rhesi*. The precipitation of calcite cement interconnects detrital particles and reduces the pore space, thus resulting in higher stiffness properties. No authigenic formation of calcite is observed at test site *Lokalbahn Salzburg*.

This study highlights the limited applicability of existing soil behaviour type charts for detecting soil structure in continental Alpine basins and emphasizes the great potential of seismic measurements to overcome these limitations. A comprehensive characterization of soil fabric and structure was carried out for Alpine lacustrine sediments, highlighting the importance of cement precipitation as a structure-forming process.

Future investigations should intend to validate and improve existing soil behaviour type charts based on high-quality field data obtained at different locations. Chamber tests should further be used to study the influence of artificial cementation on results of soil behaviour type charts under laboratory conditions. High-quality specimens should be sampled in Alpine basins to characterize the influence of soil structure on mechanical properties based on laboratory tests. We recommend that soil specimens should be characterized further by means of (transmission) electron microscopy performed at high-spatial resolution and novel, mathematical (statistical) algorithms to detect distinct changes in soil mineralogy and pore space distribution (e.g. application of artificial intelligence) with depth and age. Stable isotopes of carbon and oxygen could be investigated to assess the links between CO_2 uptake from the atmosphere and the subsequent increase in SOM content and $CaCO_3$ precipitation dynamics. Such multi-analytical approaches will contribute to develop a better understanding of the influence of soil fabric and soil structure on its stiffness and strength properties.

Author contribution SO, LH and AB contributed to the conceptualization methodology and writing—original draft preparation; SO, LH, AB and MN were involved in the formal analysis and investigation; RM, FT, HFS, MN and MD assisted in the writing—review and editing; SO, LH and RM contributed to the funding acquisition; RM, FT

and MD were involved in the resources; RM, FT and AB assisted in the supervision.

Funding Open access funding provided by Graz University of Technology. This research was funded by the Austrian Research Promotion Agency (FFG, grant number FO999891282).

Data availability Some or all data, models, or codes that support the findings of this study are available from the corresponding author upon reasonable request.

Declarations:

Conflict of interest The authors declare no competing interests, and the manuscript is approved by all the authors for publication. The authors would like to declare that the work described was original research that has not been published previously, and not under consideration for publication elsewhere, in whole or in part.

Ethical approval This article does not contain any studies with human participants or animals performed by any of the authors.

References

Arroyo M (2001) Pulse tests in soil samples. Dissertation, University of Bristol

Arroyo M, Pineda JA, Romero E (2010) Shear wave measurements using bender elements in argillaceous rocks. Geotech Test J 33(6):102872. https://doi.org/10.1520/GTJ102872

ASTM D2487-17e1 (2017) Practice for Classification of Soils for Engineering Purposes (Unified Soil Classification System). West Conshohocken, PA

ASTM D5778-12 (2012) Test Method for Electronic Friction Cone and Piezocone Penetration Testing of Soils. West Conshohocken, PA

ASTM D7400/D7400M-19 (2019) Standard Test Methods for Downhole Seismic Testing. West Conshohocken, PA

Bahlburg H, Dobrzinski N (2011) A review of the Chemical Index of Alteration (CIA) and its application to the study of Neoproterozoic glacial deposits and climate transitions. Geol Soc Lond Mem 36(1):81–92. https://doi.org/10.1144/M36.6

Baldermann A, Abdullayev E, Taghiyeva Y, Alasgarov A, Javad-Zada Z (2020a) Sediment petrography, mineralogy and geochemistry of the Miocene Islam Dağ Section (Eastern Azerbaijan): implications for the evolution of sediment provenance, palaeo-environment and (post-)depositional alteration patterns. Sedimentology 67(1):152–172. https://doi.org/10.1111/sed.12638

Baldermann A, Dietzel M, Reinprecht V (2021) Chemical weathering and progressing alteration as possible controlling factors for creeping landslides. Sci Total Environ 778:146300. https://doi.org/10.1016/j.scitotenv.2021.146300

Baldermann A, Mittermayr F, Bernasconi SM, Dietzel M, Grengg C, Hippler D, Kluge T, Leis A, Lin K, Wang X, Zünterl A, Boch R (2020) Fracture dolomite as an archive of continental palaeoenvironmental conditions. Commun Earth Environ. https://doi.org/10.1038/s43247-020-00040-3

Burland JB (1990) On the compressibility and shear strength of natural clays. Géotechnique 40(3):329–378. https://doi.org/10.1680/geot.1990.40.3.329

Collins K (1983) Scanning electron microscopy of engineering soils. Geoderma 30(1–4):243–252. https://doi.org/10.1016/0016-7061(83)90070-8

Cotecchia F, Chandler RJ (2000) A general framework for the mechanical behaviour of clays. Géotechnique 50(4):431–447. https://doi.org/10.1680/geot.2000.50.4.431

Cotecchia F, Cafaro F, Aresta B (2007) Structure and mechanical response of sub-Apennine blue clays in relation to their geological and recent loading history. Géotechnique 57(2):167–180. https://doi.org/10.1680/geot.2007.57.2.167

DeJong JT, Gomez MG, San Pablo ACM, Graddy CMR, Nelsen DC, Lee M, Ziotopoulou K, El Kortbawi M, Montoya B, Kwon TH (2022) State of the art: MICP soil improvement and its application to liquefaction hazard mitigation. In: Proc 20th ICSMGE

Eslaamizaad S, Robertson PK (1996) Seismic cone penetration test to identify cemented sands. In: Proc 49th Can Geotech Conf. pp 352–360

Fearon RE, Coop MR (2000) Reconstitution: What makes an appropriate reference material? Geotechnique 50(4):471–477. https://doi.org/10.1680/geot.2000.50.4.471

Fonseca AVd, Pineda JA (2017) Getting high-quality samples in 'sensitive' soils for advanced laboratory tests. Innov Infrastruct Solut 2(1):1108. https://doi.org/10.1007/s41062-017-0086-3

Garrett AB (1963) Carbon-14 dating: Willard F .Libby. J Chem Educ 40(2):76. https://doi.org/10.1021/ed040p76

Geomil equipment (2021) Ranger-46/66 Soil Sampling System. https://www.geomil.com/products/ranger-46-66

Geomil equipment (2022) Fox-150: Modular stand-alone CPT system. https://s3.eu-central-1.amazonaws.com/z3r2zxopa4uuqpw5a4ju/geomil/files/Geomil_Fox-series_150and200.pdf

Goldberg K, Humayun M (2010) The applicability of the Chemical Index of Alteration as a paleoclimatic indicator: an example from the Permian of the Paraná Basin, Brazil. Palaeogeogr Palaeoclimatol Palaeoecol 293(1–2):175–183. https://doi.org/10.1016/j.palaeo.2010.05.015

Goto S, Suzuki Y, Nishio S, Ohoka H (1992) Mechanical properties of undisturbed Tone-River gravel obtained by in-situ freezing method. Soils Found 32(3):15–25. https://doi.org/10.3208/sandf1972.32.3_15

Hauser L, Schweiger HF (2021) Numerical study on undrained cone penetration in structured soil using G-PFEM. Comput Geotech 133(3):104061. https://doi.org/10.1016/j.compgeo.2021.104061

IRTP (1999) ISSMGE Technical Committee TC16 Ground Property: International Reference Test Procedure (IRTP) for the Cone Penetration Test (CPT) and the Cone Penetration Test with pore pressure (CPTU). In Proc. 12th ECSMGE, 2195–2222

ISO 14688-1 (2017) Geotechnical investigation and testing - Identification and classification of soil—Part 1: identification and description. Geneva

ISO 22476-1 (2012) Geotechnical investigation and testing - Field testing - Part 1: Electrical cone and piezocone penetration test. Geneva

Jamiolkowski M, Ladd CC, Germaine JT, Lancellotta R (1985) New developments in field and laboratory testing of soils. In Proc. 11th ICSMFE, 57–153

Lee JS, Santamarina JC (2005) Bender elements: performance and signal interpretation. J Geotech Geoenviron 131(9):1063–1070. https://doi.org/10.1061/(ASCE)1090-0241(2005)131:9(1063)

Leroueil S, Vaughan PR (1990) The general and congruent effects of structure in natural soils and weak rocks. Géotechnique 40(3):467–488. https://doi.org/10.1680/geot.1990.40.3.467

Marchetti S, Monaco P, Totani G, Marchetti D (2008) In situ tests by seismic dilatometer (SDMT). In: Proc ASCE Geotechnical Special Publication honoring Dr. John H. Schmertmann: From research to practice in geotechnical engineering. pp 292–311

Marte R, Oberhollenzer S (2022) Schadensbeispiele an Bauwerken in weichen Böden - Ursachen und Erfahrungen. In Proc. Geotechnik Schweiz - Frühjahrstagung

Mitchell JK (1976) Fundamentals of soil behavior. Wiley, Toronto

Moore DM, Reynolds RC (1997) X-ray diffraction and the identification and analysis of clay minerals. Oxford University Press, Oxford

Nesbitt HW, Young GM (1982) Early Proterozoic climates and plate motions inferred from major element chemistry of lutites. Nature 299(5885):715–717. https://doi.org/10.1038/299715a0

Nespereira J, Blanco JA, Suárez M, García-Romero E, Yenes M, Monterrubio S (2021) Structure and mechanical properties of the dueñas clay formation (Tertiary Duero Basin, Spain): An overconsolidated clay of lacustrine origin. Appl Sci 11(24):12021. https://doi.org/10.3390/app112412021

Nishi K, Ishiguro T, Kudo K (1989) Dynamic properties of weathered sedimentary soft rocks. Soils Found 29(3):67–82. https://doi.org/10.3208/sandf1972.29.3_67

Oberhollenzer S, Baldermann A, Marte R, Tahir DMM, Tschuchnigg F, Dietzel M, Nachtnebel M (2022a) Microstructure development in artificially cemented. Fine-Grained Soils Geosci 12(9):333. https://doi.org/10.3390/geosciences12090333

Oberhollenzer S, Hauser L, Brand F, Marte R, Schweiger HF (2022b) Characterization of young sediments using CPTu and Medusa SDMT. In Proc. CPT22, 617–622

Oberhollenzer S, Marte R, Gasser D, Premstaller M, Leitich A (2019) Mikrostruktur des Salzburger Seetons – Charakterisierung basierend auf Drucksondierungen. Geomech Tunn 12(4):340–351. https://doi.org/10.1002/geot.201900012

Petry TM, Little DN (2022) Review of stabilization of clays and expansive soils in pavements and lightly loaded structures—history, practice, and future. J Mater Civ Eng 2022:447–460

Robertson PK (2009) Interpretation of cone penetration tests—a unified approach. Can Geotech J 46(11):1337–1355. https://doi.org/10.1139/T09-065

Robertson PK (2016) Cone penetration test (CPT)-based soil behaviour type (SBT) classification system—an update. Can Geotech J 53(12):1910–1927. https://doi.org/10.1139/cgj-2016-0044

Schmertmann JH (1991) The mechanical aging of soils. J Geotech Eng 117(9):1288–1330. https://doi.org/10.1061/(ASCE)0733-9410(1991)117:9(1288)

Schnaid F (2009) In situ testing in geomechanics—the main tests. Taylor & Francis Group, London

Steindl FR, Baldermann A, Galan I, Sakoparnig M, Briendl L, Dietzel M, Mittermayr F (2019) Chemical resistance of eco-concrete—experimental approach on Ca-leaching and sulphate attack. Constr Build Mater 223:55–68. https://doi.org/10.1016/j.conbuildmat.2019.06.189

Tavenas F, Leroueil S (1980) The behavior of embankments on clay foundations. Can Geotech J 17(2):236–260. https://doi.org/10.1139/t80-052

van Husen D (1979) Verbreitung, Ursachen und Füllung glazial übertiefter Talabschnitte an Beispielen in den Ostalpen. EGQSJ 29:9–22

Wang Y, Benahmed N, Cui Y-J, Tang AM (2017) A novel method for determining the small-strain shear modulus of soil using the bender elements technique. Can Geotech J 54(2):280–289. https://doi.org/10.1139/cgj-2016-0341